Modeling kinetics-transport interactions during biomass torrefaction: The effects of temperature, particle size, and moisture content

Citation: Bates, Richard B., and Ahmed F. Ghoniem. "Modeling Kinetics-Transport Interactions During Biomass Torrefaction: The Effects of Temperature, Particle Size, and Moisture Content." Fuel 137 (December 2014): 216–229.

As Published: http://dx.doi.org/10.1016/j.fuel.2014.07.047

Publisher: Elsevier

Persistent URL: http://hdl.handle.net/1721.1/105475

Version: Author's final manuscript: final author's manuscript post peer review, without publisher's formatting or copy editing

Modeling kinetics-transport interactions during biomass torrefaction

Richard B. Bates and Ahmed F. Ghoniem

Department of Mechanical Engineering, Massachusetts Institute of Technology, Cambridge, MA

ABSTRACT:

A comprehensive one-dimensional model accounting for the effects of heat and mass transfer, chemical kinetics, and drying was developed to describe the torrefaction of a single woody biomass particle. The thermochemical sub-models depend only on previously determined or measured characteristics, avoiding the use of fitting or tuning parameters and enabling a rigorous energy balance of the process. Moreover, a high temperature drying sub-model is introduced which overcomes the difficulties associated with existing approaches to give physically consistent results, smooth implementation, and numerical stability. The particle model was validated against experimental data from the literature for intraparticle temperature profiles, particle mass and energy yields over a range of particle sizes and reaction temperatures. The modeling results describe well the three distinct stages observed during the torrefaction of large particles including the heatup, drying, heat release due to exothermic reactions resulting in thermal overshoot, followed by thermal equilibrium where conversion is governed by mass loss kinetics. The nonlinear effects of particle size, temperature, moisture content, and residence time on the mass and energy yields are quantified and explained. Larger particles exhibit a significant internal temperature gradient and strong temperature overshoot especially at the centerline. The magnitude of the overshoot is a function of the conductivity, particle size, and average heat release rate. Because of the rise in the reaction rate, higher temperatures increase the sensitivity of the process to particle size. Due to the dependence of drying rate on heat transfer limitations, the sensitivity of torrefaction to initial moisture content increases strongly with particle size.

Highlights:

- 1D coupled model describes the dynamics of drying and torrefaction of a single particle
- Model predicts particle temperature overshoot, elemental, and energy balance
- Validated against single particle experimental results from literature
- Larger particles convert more non-uniformly with higher thermal overshoot.
- Higher temperatures and increased moisture content exacerbate particle size effects

Keywords: biomass; pyrolysis; torrefaction; modeling; heat and mass transfer

Corresponding Author: Richard B. Bates
Address: Room 3-339 77 Massachusetts Avenue Cambridge, MA 02139 USA
Email: rbates@mit.edu
Telephone: +1 617 253 5365
Fax: +1 615-253-5981

Second Author: Professor Ahmed F. Ghoniem
Address: Room 3-344 77 Massachusetts Avenue Cambridge, MA 02139 USA
Email: ghoniem@mit.edu Telephone: +1 617 253 5981

1. **Introduction**

Because of increasing concerns over rising greenhouse gas emissions, biomass has received interest as a renewable feedstock for a variety of thermochemical processes including combustion, gasification, and pyrolysis. However raw biomass displays several unfavorable properties related to its low bulk energy density, high moisture content and uptake rate, and exorbitant size reduction energy penalty. Torrefaction has been proposed and studied as thermal pretreatment approach to improve these characteristics [1,2]. Torrefaction is a mild pyrolysis process occurring between 200-300 $^{\circ}$C over a residence time between several minutes to about an hour which results in partial devolatilization (0-60% by weight) of the original dry feedstock [3]. During torrefaction, the release of the volatiles combined with other changes to the physical and chemical structure result in a solid product with greater specific energy density, increased resistance to fungal degradation [4], and reduced grinding energy requirement [5].

Torrefaction is a complex process involving coupled intraparticle physical and chemical phenomena including external heat transfer, intraparticle heat transfer, thermochemical decomposition, convection and diffusion of volatile products. For sufficiently small particles (<2mm), torrefaction is essentially free of heat and mass transfer limitations [6,7]. The solid mass loss kinetics of torrefaction in this regime has been studied for a variety of woody feedstocks including willow [6], beech [8] and softwoods (pine, fur, spruce, and pine bark)[9]. The torrefaction of the individual lignocellulose components (xylan, cellulose, and lignin) has also been examined [10].

Because of the high grinding energy requirement of raw biomass [5], industrial scale torrefaction will preferably be performed with large (>2mm) particles. In this case, significantly more complex interactions occur. Heat transfer limitations cause a temperature gradient across

the particle resulting in chemical reactions proceeding non-uniformly. The non-uniform release of heat due to exothermic decomposition reactions can further exacerbate the heterogeneity of the process and even lead to thermal runaway [8,11] . In order to examine these phenomena, robust coupled transient models describing the transport, kinetics, and thermochemistry are required. Numerous 1D and 2D physico-chemical models exist in the literature that describe single particle pyrolysis at high temperatures (400-700 $^{\circ}$C) [12–16]. However, compared to torrefaction, pyrolysis at these high temperature results in partial to complete devolatilization (70-90 wt%) and different thermal degradation pathways are expected.

Fewer models have considered coupled heat/mass transfer and kinetics at low temperatures (<300 $^{\circ}$C) consistent with torrefaction. Turner and coworkers [11,17] developed a 2-D computational heat and mass transfer model for the torrefaction of beech (*Fagus sylvatica*) wood and compared the predicted temperature profiles to experimental results using large (5 x 15 x 25cm) beech boards. Their assumed kinetic mechanism described wood thermal decomposition as a linear superposition of the decomposition hemicelluloses, cellulose, and lignin components. Turner noted that the reaction enthalpy term has a very important effect on the temperature profiles[17], however due to the lack of available parameters in the literature, the enthalpy of reaction of the hemicellulose decomposition was used as a tuning parameter. Kadem and coworkers [18] developed a transient 3-D computational model of the heat treatment (150-250 $^{\circ}$C) of wood, focused on heat and moisture transfer (drying), and neglected thermal decomposition kinetics. Patuzzi and coworkers developed and validated a model describing the heat, mass, and momentum transfer during the torrefaction of common reed (*P. australis*) in a custom bench-scale reactor[19]. Parameters for a two stage solid mass-loss kinetics mechanism were separately fitted, and the global heat of reaction (including both drying and torrefaction)

was treated as a calibration parameter. Ratte et al. developed a particle-scale model coupled with a reactor model to describe their laboratory pilot (3-8 kg/hr) moving bed reactor system [20,21]. They adopted a global kinetics decomposition model while the thermochemical model postulated a fixed composition of solid and volatile products enabling them to explicitly model their enthalpies. Although the particle sub-model [20] was not compared explicitly with experimental particle temperature profiles, the reactor model was validated against measured gas temperature profiles [21]. Recently, Basu and coworkers [22] compared a 1D particle scale model with experimental measurements of solid mass loss curves and centerline temperature profiles from cylindrical poplar dowels. While the solid mass loss kinetics of the first stage were separately fitted under TGA conditions, multiple kinetic and thermochemical parameters were tuned during the development of the particle scale model including the heat of reaction. In reviewing the previous modeling efforts, no models exist which simultaneously i) show detailed validation with intraparticle temperatures, ii) are free of tunable parameters, iii) give information on the energy yield of the solid product.

In this paper, we formulate a particle scale model that couples drying, torrefaction kinetics, and relevant transport processes which overcomes these aforementioned deficiencies. Ultimately, the model is then used to examine the effects of particle size, temperature, and moisture content on the overall rate and uniformity of the process. We use previously determined thermochemical and kinetic data and validate the model against published experimental data. In such a way, the model is formulated without the use of adjustable or fitting parameters. In the first part of this paper, a characteristic time scale analysis is applied to identify the dominant physical and chemical phenomena occurring during torrefaction of large particles. Next, the mathematical formulation of the coupled transport and kinetics model is presented

along with the selected kinetics and thermochemistry model. In the following section, the results are validated against the experimental measurements of van der Stelt [8] and Basu [23]. The discussion highlights the models ability to capture important behaviors occurring during single particle torrefaction including the effects of particle size, moisture content, temperature, and exothermic overshoot.

2. **Physical and chemical processes during torrefaction**

Biomass particles undergoing torrefaction experience a complex set of interacting phenomena including mass and heat transfer as well as drying and chemical devolatilization. It is important to judiciously identify the most relevant processes in order to formulate representative models.

2.1.Drying

Drying is one of the first processes to occur during the torrefaction of a biomass particle and represents a significant thermal load during the process. Moisture present in fresh wood varies between 15-60% by mass on a wet basis (w.b.) depending on the type, location and method of storage[24,25]. Even after the application of a thermal drying process, the equilibrium moisture content will still remain above 6-10% w.b. depending on the relative humidity and temperature [26–28]. Water exists in three forms within biomass including i) vapor, ii) free (or capillary) water, and iii) bound (or hygroscopic) water [27]. Bound water is adsorbed through hydrogen bonding [29] to the cell wall constituents (hemicelluloses, cellulose). Once the adsorption sites are saturated with bound moisture, the fiber saturation point is reached (typically 23% w.b. or 30% d.b.)[24]. Above this moisture content, water fills the voids or pores of the biomass and is referred to as free water.

During torrefaction, free and bound moisture can be completely evaporated and resulting in a product with as low as 0-2% moisture [30]. Additionally, the decomposition of hydroxyl

groups in the cell wall components resulting in a more hydrophobic product [31,32]. While the effect of initial moisture content on the torrefaction process has yet to be studied experimentally, drying has previously been shown to affect pyrolysis times [27]. Because of the large latent heat of vaporization of liquid moisture, the thermal load associated with drying -even for a relatively dry particle of 6% w.b.- will be significant (~30%) compared to the sensible heat required to raise the temperature of the particle from ambient to reaction temperatures (200-300 $^{\circ}$C).

The dominant drying mechanisms depend on temperature and can include bulk convective and diffusive flow of free and bound moisture. Under high temperature drying conditions (>100 $^{\circ}$C) the diffusive flow of bound moisture and vapors can be considered negligible compared to the convective flow of vapor [33,34] .

2.2.Characteristic time scale analysis

A characteristic time scale analysis similar to that performed by Chan et al. [12] aids in identifying the dominant processes occurring during the drying and torrefaction of a single particle and is summarized in Table 1. Although, the time scales do not represent the magnitude of the driving forces behind such processes (i.e temperature gradient) they allow the identification of the rate controlling mechanisms. The analysis provides justification for the approximations and assumptions made in the mathematical model presented next. Values for wood and gas physical properties - including conductivity (k), specific heat (c_p), and density (ρ)- were taken from [35]. The value for the diffusivity (D), was estimated by the correlation in [29] while permeability (B_0), and gas viscosity (μ) were taken from [15]. The solid mass loss reaction rate was evaluated with the willow mass loss kinetics at 300 $^{\circ}$C [3] and the drying rate was evaluated at 100°C[36]. The length scales described in Table 1 include micro scale, which

corresponds to the pore diameters, and macro scale- reflecting the maximum size of feed particles.

Several important observations can be drawn from Table 1. Mass transfer, especially pressure-driven transfer, occurs at time scales much faster than either heat transfer or reactions. At the micro scale of the wood pores (tracheids), convective heat transfer is rapid compared to kinetics, and the heat capacity of gas is low compared to the heat capacity of the solid. As a result, gas leaving the solid rapidly heats up to the temperature of the wood/char it flows through. If a positive temperature gradient exists in the particle, these outward flowing volatiles can cool the outer hotter layers as they leave. This effect is often neglected for simplicity [22,35,37] but has been shown to be significant, especially during drying [13,33]. The relative importance of the convective term to the internal conduction term can be quantified by the relevant Peclet number. Under conditions of active drying or devolatilization, the Peclet number has an order of magnitude of 1, confirming that the heat transfer associated with the flowing volatiles should be included.

$$Pe = L\rho_g cp_g u / k_{solid} \quad (1)$$

Considering the characteristic length scale of relatively large particles (L=0.01m), drying, mass loss kinetics, external heat transfer (convection), and conduction have time scales of similar order of magnitude. Therefore no rate-limiting simplifications can be made and the model must account for these transport mechanisms.

A summary of the conclusions derived from Table 1 :

(1) Mass transfer via diffusion is much slower than that by hydrodynamic (pressure driven) flow from drying or devolatilization.

(2) Mass transport by convection is rapid and occurs much faster than heat transport, drying, and chemical devolatilization processes.

(3) The thermal heat capacity of the gas $\left(\rho c_p\right)_{\mathrm{g}}$ is much less than that of the solid $\left(\rho c_p\right)_{\mathrm{s}}$. As a result local thermal equilibrium exists between the volatiles and the solid. Internal convective heat transfer is significant under conditions of active devolatilization.

3. **Mathematical model**

The formulation of the numerical model is based on the following assumptions:

(1) Particles are represented in a one-dimensional, time-dependent domain. A shape factor enables the description of slab, cylinder, or spherical geometries.

(2) Total volume of the particle remains unchanged during torrefaction. In other words, no overall structural changes (i.e shrinkage, breakage) occurs.

(3) Outflow of volatiles is instantaneous such that the pressure of the particle remains unchanged during drying and torrefaction.

The physical processes described by the model include:

(1) Heat transfer by radiation, convection, and conduction to the exposed surfaces of the particle and within the solid.

(2) Convective mass transport of the volatiles through the particle

(3) Variable thermal properties (moisture content, conductivity, density, heat capacity)

Biomass is inherently anisotropic with the properties like thermal conductivity and permeability being especially dependent on the grain orientation[29]. However, the assumption of one-dimensionality along with an effective set of physical properties is valid and commonly made in the literature[15,34,37–40] during the uniform heating of cylindrical biomass particles of

sufficiently long aspect ratio. Acceptable agreement between 1D models and experimental data with cylindrical particle aspect ratios as low as 2 for Di Blasi & Galgano [39], 5-8 for Lu [15] and 2.7 for Pyle & Zaror [37]. Alves & Figueiredo [34] found that beyond an aspect ratio of 3, the pyrolysis time was hardly affected.

3.1.Drying

Three existing modeling approaches have been applied for estimating the evaporation rate of large biomass particles undergoing high temperature drying, pyrolysis, or combustion. These include the i) first order kinetic evaporation model [12,33,36,41–43], ii) equilibrium model [29,44–46], and iii) a constant temperature model (also known as the heat sink model)[34,39,40,47–49]. The first order kinetic approach is a simplified approach which treats the evaporation rate as a thermally activated process described with a first order Arrhenius rate equation. The activation energy and pre-exponential factor are chosen to produce an evaporation rate which increases rapidly at the boiling temperature [33,50]. The advantages of this method are that it is implemented easily as an additional chemical reaction in particle models and results in smooth intraparticle gradients[51]. The disadvantages are that some drying occurs before the boiling temperature is actually reached, and the kinetic parameters in the literature show a wide scatter [52].

The equilibrium approach accounts for heat and mass transfer limitations and assumes that the bound and free liquid moisture exist in equilibrium with the local gas phase. The partial pressure of water vapor is fixed by the local saturation pressure. The disadvantage of the equilibrium approach is that it is known to result in depressions in pressure in locations ahead of the drying front and requires simultaneous solution of algebraic and differential equations [51].

The heat sink approach assumes that drying is controlled entirely by heat transfer: when a moist particle layer has reached the boiling temperature (e.g. 100 $^{\circ}$C), all energy flowing into that layer is consumed entirely by evaporation of water until drying ceases. It is implemented in models in one of two ways. Either the drying front is assumed to be infinitely thin and the particle is divided into moist and dry sections or the governing equations must include a conditional statement. The former method, though easily implemented, is not necessarily valid in cases where the drying front has a thickness comparable to the particle[43]. The latter method requires special numerical treatment and is not computationally efficient due to the sharp discontinuities it introduces into the governing equation [51,52].

In the current model, an approach which combines aspects of the existing methods is adopted where the drying rate is evaluated by a first order Arrhenius equation but has a conditional dependence on temperature (see equation (**6**). The drying rate is set to 0 for temperatures below the boiling temperature. As done by Bilbao and Alves & Figueiredo [34,48] who adopted the heat sink approach, the boiling temperature is set by the local moisture content and is fitted to data from [53]. This approach solves two major drawbacks of the first order Arrhenius approach. The drying profile is more physical because drying does not occur until the boiling temperature is actually reached. Also, it is less sensitive to the assumed kinetic parameters because the boiling temperature is specified. At the same time, it is extremely easy to implement as an additional chemical reaction without modifying governing equations and does not entail the solution of additional algebraic equations.

3.2.Solid mass loss kinetics

A variety of models have been proposed and verified to describe the mass loss kinetics of during torrefaction. Approaches to modeling the mass loss kinetics can be divided into two main groups.

One approach is to describe the wood/biomass as three independently reacting constituents (hemicelluloses, cellulose, and lignin) [17,21]. This approach is adopted when ease of application to different feedstocks is the goal. Nocquet et al. recently assessed the additive approach and found that it reproduces solid mass loss curves up to temperatures of 250 °C; however, above this tempeature, significant interactions between the constituents were apparent-resulting in a large discrepancy[54]. The second more common approach is a lumped approach where the wood is modeled as one or multiple solid pseudophases reacting to volatiles and char. Several authors [8,9,55] have found that wood torrefaction could be modeled with two independently reacting components forming two volatile phases and two char phases. The mechanism adopted in the present study was originally proposed by Di Blasi [56] to describe hemicellulose (xylan) mass loss kinetics but was later fitted to satisfactorily describe willow[3], common reed[19], eucalyptus, and spruce[55] for temperatures up to 300°C. In this mechanism, the torrefaction products are lumped into five pseudo-components and decompose according to first order kinetics in two steps with the first step being much faster than the second as follows:

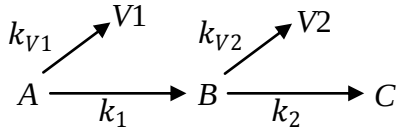

where the solid phase pseudo components (*A*,*B*,*C*) represent raw biomass (*A*), an intermediate solid (*B*), and char (*C*), volatile products are represented by *V*1 and *V*2, and k_1, k_2, k_{V1}, k_{V2} represent Arrhenius kinetic parameters.

$$k_i = A_i \, exp(-E_i/RT) \qquad (2)$$

The pre-exponential factor has units of s^{-1}, the activation energy has units of J mol^{-1}, R is the universal gas constant in J mol^{-1} $K^{-1,}$ and T is temperature in K. See **Table 2** for the parameters. It was shown that the composition of the lumped volatile pseudo-phases (V1 and V2) were

individually well described as mixture of nine identifiable chemicals: acetic acid, water, formic acid, methanol, lactic acid, furfural, hydroxyacetone, carbon dioxide and carbon monoxide[57] . See Table 2 in [57] for the details of these compositions. The advantage of this kinetic mechanism and set of parameters is that all pseudo-components (A,B,C,V1,V2) have well-defined chemical compositions thus enabling estimation of their thermodynamic properties, namely their heat of formation and specific heat capacity [58]. Thus, the elemental balance enables the estimation of the solid product composition and energy yield [59] not considered in previous single particle models.

3.2.1. **Conservation of species/mass**

The equations describing the evolution of the solid pseudo components (A,B,C) and liquid moisture (MC) are:

$$\frac{d\rho_A}{dt} = -(k_1 + k_{V1})\rho_A \tag{3}$$

$$\frac{d\rho_B}{dt} = k_1\rho_A - (k_2 + k_{V2})\rho_B \tag{4}$$

$$\frac{d\rho_C}{dt} = k_2\rho_B \tag{5}$$

$$\frac{d\rho_{MC}}{dt} = -k_d\rho_{MC}, if\ T > T_b \tag{6}$$

where ρ_i is the apparent density of pseudo component (i= A,B,C, MC) in (kg m^{-3}) and T_b is the vaporization temperature. The conditionality of the evaporation rate on temperature prevents drying from occurring before the boiling temperature has been reached. The dependence of vaporization temperature on the dry basis moisture content is fitted to the data from Alverez Noves [53]. The local dry basis moisture fraction is given by,

$$MC_d = \frac{\rho_{MC}}{\rho_S} = \frac{\rho_{MC}}{\rho_A + \rho_B + \rho_c}. \tag{7}$$

The total solid phase (dry) is modeled as a mixture of the three solid pseudo components,

$$\frac{d\rho_S}{dt} = \frac{d\rho_A}{dt} + \frac{d\rho_B}{dt} + \frac{d\rho_C}{dt} = -(k_{V1}\rho_A + k_{V2}\rho_B) \tag{8}$$

The elemental composition (i.e. the mass fraction of carbon, hydrogen, oxygen, nitrogen and ash) of the solid phase on a dry basis is given by,

$$\frac{d(m_s Y_{j,S})}{dt} = -k_{V1} m_A Y_{j,V1} - k_{V2} m_B Y_{j,V2}, \tag{9}$$

where, m_S is the mass of the solid (in kg), $Y_{j,i}$ is the mass fraction of elemental species "j" (j=C,H,O,N,Ash) contained in component "i" (e.g. S, V1, V2). See Table 2 of [57] for these mass fractions. The conservation of mass on the total gas phase is given by,

$$\frac{\partial(\varepsilon\rho_g)}{\partial t} + \frac{1}{r^n}\frac{\partial}{\partial r}\left(r^n \rho_g v\right) = -\frac{\partial \rho_s}{\partial t} - \frac{\partial \rho_{MC}}{\partial t} = k_{V1}\rho_A + k_{V2}\rho_B + k_d \rho_{MC}, \tag{10}$$

where n is a shape factor describing the particle n=1,2,3 for a slab, cylindrical, and spherical geometries. As was previously done in several other single particle pyrolysis models [12,34,60], the mass flux of volatiles (kg/m^{2}s) can be evaluated from this equation because of the assumption of fast volatile release which results in a negligible accumulation term:

$$\rho_g v = \frac{1}{r^n}\int_0^R r^n (k_{V1}\rho_A + k_{V2}\rho_B + k_d \rho_{MC}) dr. \tag{11}$$

3.3. Conservation of energy

The conservation of energy for the solid phase accounts for accumulation, conduction convection, and reaction,

$$\frac{\partial T}{\partial t}\left(\rho_A c_{p,A} + \rho_B c_{p,B} + \rho_C c_{p,C} + \varepsilon\rho_g cp_g\right) = \frac{\partial T}{\partial r}\left(\frac{\partial k}{\partial r} + \frac{kn}{r} - v\rho_g cp_g\right) + k\frac{\partial^2 T}{\partial r^2} - \dot{Q}_r, \tag{12}$$

Where the heat of reaction term,

$$\dot{Q}_r = \sum_{i=A,B,C,V1,V2} \frac{\partial \rho_i}{\partial t} H_i - \frac{\partial \rho_{MC}}{\partial t}\Delta H_{evap}, \tag{13}$$

includes the heat of vaporization ΔH_{evap} of liquid moisture in J kg^{-1}. Due to the heat of sorption of bound moisture, the heat of vaporization term shows a dependence on dry basis moisture

content [29,48] (see Table 2). The total enthalpy at temperature T is given by the summation of the formation enthalpy and sensible enthalpy,

$$H_i(T) = H_{f,i}^{\circ} + \int_{T_0}^{T} c_{p,i}\,(T)dT, \tag{14}$$

where $H_{f,i}^{\circ}$ is the standard heat of formation of species i in J/kg and $c_{p,i}$ is the specific heat capacity of component i in J kg^{-1} K^{-1}, T is the reaction temperature in Kelvin, and T_0 is the standard temperature (298.15K). The total gas phase and V1 and V2 are assumed to behave as an ideal gas mixture of their nine constituent species. Thermodynamic properties of the solid phases (A,B,C,S) and V1 and V2 are summarized in Table 2. For further information on the thermodynamic property estimation of the solid and volatile products see [58]. The effective conductivity of the solid matrix described in Table 2 includes a contribution from radiation heat transfer through the pore spaces [12] as wells as a contribution from the moisture[43,48].

3.4.Initial and boundary conditions

The initial conditions for $t = 0$:

$$T = T_0, \quad \rho_A = \rho_{A0}, \quad \rho_B = \rho_C = 0, \quad m_s Y_{j,S} = m_{s0} Y_{j,S0} \tag{15}$$

The initial chemical composition of the particle ($Y_{C,S0}, Y_{H,S0} \ldots Y_{Ash,S0}$) are summarized in **Table 2.**

The Neumann boundary conditions for $t > 0$ at the centerline r=0 reflect symmetry,

$$\frac{\partial T}{\partial r} = 0. \tag{16}$$

The Neumann boundary conditions at the surface of the particle r=R includes both convective and radiative heat transfer,

$$k\frac{\partial T}{\partial r} = h_c(T - T_r) + \omega\sigma\left(T^4 - {T_r}^4\right), \tag{17}$$

where h_c is the convective heat transfer coefficient in W m^{-2} K^{-1} and T_r is the reactor temperature in K. For the axial flow of air over stationary cylinders the heat transfer coeffient can be estimated using the correlation by Nowak and Stachel [61],

$$Nu = \frac{h_c d_p}{k_{gas}} = 0.87 {Re_p}^{-0.52} + 1.75 {Re_p}^{0.21} + 0.5 * \left(0.5 {Re_p}^{4.75} + 8 * 10^{-9} {Gr_p}^{4.24}\right)^{0.08}, \quad (18)$$

where Re_p and Gr_p represents the Reynolds and Grashof numbers, respectively, for the particle. This correlation is valid for $2<Re_p<1000$ and $0<Gr_p<10^7$. Other correlations exist in the literature for other 1D geometries (i.e sphere, slab)[15]. The temperature profile of the reactor is not coupled with the particle and is prescribed according the conditions of the particular case of interest. In the case of van der Stelt's experiments, the reactor temperature increased at a heating rate between 8-16 K/min until reaching the final temperature after which it remained constant [8]. In Basu's experiments [23] the particles were dropped into an already heated reactor.

3.5. Numerical method

The system of partial differential equations is solved using the method of lines approach where finite differences are used to approximate the spatial derivatives. The resulting system of ordinary differential equations is integrated using ode15s in MATLAB. Treatment is required for the Heaviside step function introduced by the conditionality of evaporation rate on temperature. An error function was chosen to approximate the step function which was found to provide good accuracy while having a minimal impact on the integration time.

4. Results and discussion

4.1. Comparison with the experiments of van der Stelt

van der Stelt performed torrefaction experiments using large cylindrical beech and willow particles with diameters between 1-2.8 cm and lengths of 10cm. The particles were placed in a vertical split tube oven which was electrically heated. Argon was used as an inert gas to remove

the produced volatiles from the reactor. Five thermocouples embedded inside the particle continuously monitored the temperature at radial positions (r=0, 0.3, 0.7, 1, and 1.3 cm). The particle and reactor- initially at ambient temperature- were heated at a rate of approximately 10 $^{\circ}$C/min to the final reactor temperature, which was varied between 230-300 $^{\circ}$C. The mass and/or energy yield of the particle was not reported. The initial moisture content of the particles was reported as approximately 6%.

4.1.1. **Intraparticle temperature profiles**

In Figure 1a,c) the experimentally measured temperature profiles of the beech particle at two radial positions (r=0 and r=0.013cm) are compared with the model predictions for two reactor temperatures, 235 and 289 $^{\circ}$C, respectively. Hereafter these positions are referred to as the centerline (r=0) and the near surface (r=0.013cm) positions. In both cases, the temperature of the reactor does not heat up to the final temperature in a perfectly linear fashion and for modeling the boundary conditions, the reactor profile is approximated by two separate linear heating periods. In Figure 1(a) where T_{final}=235 $^{\circ}$C, the time for the center of the particle to reach 100 $^{\circ}$C is 16.5 minutes, which is the same as the value reported in the experiment demonstrating good agreement on the initial heating period and drying dynamics. During the drying period, the temperature of the centerline of the particle is significantly higher than 100 $^{\circ}$C (the boiling temperature for liquid water at atmospheric pressure). In fact, the moisture at the centerline plateaus at ~114 $^{\circ}$C. This demonstrates that the dependence of boiling temperature on moisture content is crucial to representing the location of the drying plateau. Drying models which assume a single boiling temperature, commonly done when applying the heat-sink approach, would fail to accurately represent this characteristic. Up until 29 minutes, the modeled centerline temperature is within 3 $^{\circ}$C of the experimental data. In addition to showing quantitative

agreement with the van der Stelt's results, the drying dynamics predicted by model share qualitative similarities with previous studies focused on drying of wood cylinders. In Di Blasi's experimental study of moist (50% d.b.) pine cylinder drying at high temperatures 200-327°C [33], the evolution of the intraparticle temperature showed a period of initial heatup with low evaporation rates and relatively small particle gradients followed by a drying period where thermal gradients reached a maximum. After the centerline has finished drying, the particle then rapidly approaches the final reactor temperature. The same stages are apparent in the present results except that after drying has completed, exothermic reactions raise the centerline temperature in the model until they actually exceed the surface temperature of the particle.

The temperature profile of the near surface position (r=0.013) predicted by the model is somewhat higher than that experimentally measured profile throughout most of the period, but is within the repeatability and uncertainty range for particle temperature measurements of this type. While not reported explicitly by van der stelt, in other similar single particle experiments the uncertainty is reported to be at least $\pm 15^{\circ}$C[14]. Particularly, there is greater uncertainty near the surface of the particle where large temperature gradients exist. The thermocouple- although thin- has finite thickness (1mm) and besides the possibility that it may affect the local effective conductivity, its exact position may not be known precisely.

At the final temperature (at t=60 minutes) at the centerline is at 241 $^{\circ}$C which compares well with the experimentally measured centerline temperature of 240°C. At 60 minutes, the rate of change of temperature at the centerline and surface of the particle is small in both the model and the experiment, demonstrating that the system has reached a quasi-steady state. At this moment, the heat loss from the particle balances any heat released from reactions.

In Figure 1(b) for the case of T_{final}=289 °C, the time for the center of the particle to reach 100 °C is 13 minutes for both model and experiment, showing good agreement on the initial heating and drying period. A drying temperature plateau at the centerline is well represented by the model and occurs between 112-116 °C.

The model predicts that the centerline reaches a maximum temperature of 329°C at 38 minutes which is also in good agreement with the experimentally measured maximum temperature of 335°C at 39 minutes. The model predicts that after reaching the peak temperature, the centerline temperature decreases at a rate faster than the experiment. This is attributable to the endothermic reactions of the second stage which act to cool the particle down. As a result at t=60 minutes the predicted centerline temperature is 285 °C which is 20 degrees lower than the experimentally measured centerline temperature of 306°C. There are several reasons for this discrepancy. First, both the solid mass loss kinetics mechanism and thermochemical submodel were developed using temperature data below 300°C, specifically for willow feedstock[6,58]. This commonly used temperature limit was originally chosen to avoid excessive decomposition of the relatively carbon-rich lignocellulose components-namely cellulose and lignin) [6,57]. At temperatures exceeding 300°C, more complex degradation pathways may become significant such as exothermic char-forming reactions[62], secondary reactions between the volatiles and the char products [8] and thermal tar cracking [63]. Given the high sensitivity of the rates and degradation pathways to temperature, the application of these mechanisms 30-40 °C above the original range of fitting would strictly be considered extrapolation. Unfortunately, no high temperature (300-350°C) torrefaction mass loss kinetics mechanisms or thermochemical sub-models currently exist, so it may be suggested that future studies may consider data in this temperatures range. Secondly, in the thermochemistry

submodel adopted in this study, the heat of reaction of the slower second stage is endothermic but displays more uncertainty compared to the first stage which has been positively identified as exothermic [58]. The uncertainty arises from the variability in the heating values of the solid products as predicted by empirical correlations. It was previously suggested that better characterization of these products would help to identify whether second stage is either endothermic or exothermic; however, the under-prediction of particle temperature by the current model suggests the heat of reaction of the second stage is thermally neutral or even slightly exothermic. The sensitivity of the predicted temperature profile during this period to the mass loss kinetics and thermochemistry are agree with conclusions made from previous single-particle models[17].

Figure 1(b)(d) shows the intraparticle temperature profiles at two radial positions and three times (t=10,20,40 minutes) for the cases of final reactor temperatures of 235 and 289 $^{\circ}$C, respectively. Intraparticle temperature gradients exists because of the internal heat transfer limitations which are expected to be significant as the Biot number ($Bi=hL/k$) is of order 1. For the T_{final}=235°C case, a positive temperature gradient across the particle develops for 20 minutes and reaches a maximum during the drying stage at which point the surface of the particle is 50 degrees higher than the center. The experimental data shows that the temperature gradient remains positive throughout the entire hour. In the model the centerline temperature very slightly exceeds the surface by approximately 4°C after 40 minutes. Despite this apparent qualitative difference, the difference between the model prediction and experimental centerline temperature is within 8°C which is well within the experimental error (±15°C).

For the T_{final}=289°C case, a positive temperature gradient across the particle develops for 23 minutes where the surface of the particle is up to 85 degrees higher than the centerline. This

positive gradient vanishes by 32.5 minutes and eventually becomes significantly *negative*. In fact, the centerline becomes hotter than the surface by up to 26°C agreeing with cnterline-surface temperature overshoot of up 20 °C is apparent experiment as well. The cause for this phenomenon is the heat released from the exothermic torrefaction reactions. According to Fourier's law, this heat generated in the inner layers can only conduct towards the outer layers of the particle when a negative temperature gradient exists ($dT/dr < 0$). It is only when sufficiently *negative* temperature gradient has developed that a maximum in the centerline temperature is reached where the heat transfer by conduction and convection balances the heat released by reactions. During this period of thermal overshoot, the heat transfer by convection of hot volatiles outwards through the particle is small -but significant- and contributes to heating the outer layers.

4.1.2. **Effect of temperature**

van der Stelt repeated the experiments with the 28mm diameter beech particles at final reactor temperatures ranging between 200-280°C. In Figure 2a, model predictions for the centerline temperature overshoot are compared with the experimental results. The overshoot is defined by the largest positive temperature difference between the centerline and the reactor. At 200 °C the rate of torrefaction reactions is negligible producing few volatiles and therefore a very small (<1 °C) thermal overshoot. The magnitude of the overshoot rises rapidly with increasing temperatures and is certainly a non-linear effect. This is because the heat release and temperature are closely coupled: higher temperatures result in faster heat release increasing the temperature further. The overshoot stabilizes itself when a sufficiently negative temperature gradient exists in the particle, thereby enabling conduction of the heat outward.

Good quantitative agreement on the magnitude of the thermal overshoot as a function of temperature is reached between the model and experiment. Using a simplified particle model, van der Stelt concluded that the temperature overshoot was proportional to the average volumetric heat release rate. Based on the thermal overshoot observed in the cylindrical particles, he estimated the cumulative heat release to be less than 250 kJ/kg. The present modeling results corroborate this conclusion; the predicted cumulative heat release is less than 180 kJ/kg. As originally concluded by Turner [17] the particle temperature profile during this overshoot period is extremely sensitive to the assumed thermochemistry model. In this case, the heat of reaction was not adjusted to fit the data. Instead its value depends solely on the composition of volatile and solid products which were fitted separately in [57] and whose enthalpies were estimated in [58].

Figure 2b shows the model predictions for the final (t=60 minutes) mass/energy yield for single 28mm diameter beech wood particles as a function of reactor temperatures between 200-280 $^{\circ}$C. For a given residence time and particle size, mass and energy yields decrease with temperature. Higher temperatures result in more rapid mass loss. The highly oxygenated volatiles released during torrefaction contain less energy than the original solid product [58]. As a result the energy yield of the remaining solid product is always higher than the mass yield. This results in a product with greater energy density per unit mass. van der stelt did not measure the energy yield of the particles after the experiment so a comparison on this quantity is not available. Having thoroughly described and explained the phenomena associated with coupled thermal-kinetic effects at variable temperatures for relatively large cylindrical particles (2.8cm diameter), the next section examines and validates the model predictions for various particle sizes.

4.2. Comparison with the experiments of Basu and coworkers

Basu and coworkers performed torrefaction experiments using large cylindrical poplar (*P. deltoides*) and particles with diameters between 0.476-2.54 cm and lengths of 0.8-6.5 cm and initial moisture content of 6.39%w.b. The particles were suspended by a thermocouple from an electronic balance which monitored the weight of the sample. The thermocouple continuously recorded the temperature at the center of the particle (r=0 cm). The convective reactor was a 42mm diameter Quartz Wool Matrix reactor which was externally electrically heated. Nitrogen was used as an inert gas flowing at a rate of 1.2L/min. In each case the higher heating value of the torrefied particle after the experiment was measured using a bomb calorimeter in order to evaluate the energy yield:

$$\eta_{Energy} = \frac{m_{S,f} HHV_{S,f}}{m_{S,0} HHV_{S,0}} \tag{19}$$

Where $HHV_{S,f}$ is the final higher heating value of the torrefied particle. The mass and energy yields were only reported at the end of the experiment at 60 minutes and the effect residence time was not studied.

4.3.Effect of particle size

In Figure 3a, the model predictions for the centerline-reactor temperature overshoot as a function of particle size are compared with the experimental results from Basu et al. and Dhungana [64]. In all cases, the reactor temperature was held constant at 250 $^{\circ}$C while the initial particle temperature was approximately 25°C. The model predicts a 12.75mm radius particle would experience an overshoot of 11.1 degrees which lies almost exactly between the two experimental measurements (7, 18 $^{\circ}$C). Both data sets (Basu et al. and Dhungana) refer to the same set of experiments done by the same group but mentioned in different publications. It is presumed that

this discrepancy is because of the uncertainty on the actual reactor and particle centerline temperatures.

Nevertheless, the trend is clearly visible in both model and experimental results: the magnitude of the centerline-reactor thermal overshoot increases quadratically with particle size. The theoretical explanation for this trend was first analyzed by van der Stelt [8], where a simplified quasi-steady state analysis of the energy conservation equation **(**12**)** showed that the maximum temperature difference between the centerline and the surface of the particle should be proportional to the square of the particle radius (R in m^2), the volumetric heat *release* rate ($-\dot{Q}_r$ in W/m^3) and inversely proportional to the effective conductivity (k in $W\ m^{-1}\ K^{-1}$) that is, $\Delta T_{c-s} \propto -\dot{Q}_r R^2/k$.

Figure 3b shows the time for the centerline of the particle to heat up from its initial temperature to 200 $^{\circ}$C. This heatup time is defined this way because torrefaction reactions do not initiate until 200 $^{\circ}$C. The model predicts the heatup time within 45 seconds of the experimental values. For the largest diameter particle, the heatup period takes more than a quarter (16.5 minutes) of the total residence time of the particle (60 minutes).

The length of the heatup period is governed by two factors. The first is the rate of heat transfer to the particle which can be quantified by the characteristic time (in seconds) associated with solid particle heating. These scale linearly, $\rho c_p L/h$, or quadratically, $\rho c_p L^2/k$ with size, depending on whether the heat transfer is limited by external or internal heat transfer rates, respectively. In this case, the Bi ranges from 0.5 to 5 for the smallest particle to largest particle so that neither external nor heat transfer is rate limiting and the heatup time should be expected to scale with particle size with an order between 1-2. The second controlling factor during this period is the moisture content of the particle. It has been previously been observed that the length

of time for drying varies linearly with the initial moisture content of moist wood cylinders subjected to convective heating [33]. This occurs for several reasons: 1) liquid water has a more than double the specific heat capacity of biomass (4800 and ~2300 J/kg K, respectively), which is not offset by its contribution to increasing the effective thermal conductivity [33]. This lengthens the aforementioned characteristic times scales for heating. 2) Drying slows the particle heating rate because it is a strongly endothermic process and acts as a thermal sink. At certain locations in the particle, the thermal load for evaporation balances the rate of heat conduction inwards, and the temperature does not continue to rise until all remaining moisture has been evaporated. 3) The rapid outward convection of vapor from inner layers contributes to cooling the outer layers. Thus the ability of the model to predict heatup time well suggests that these key processes are described satisfactorily.

Figure 3c shows the model predictions for the mass/energy yields for the poplar particles of various sizes at 250 $^{\circ}$C. Experimental results from Basu et al. demonstrate that the mass and energy yields decrease slightly with increasing particle size though the significance of this trend is not clear[64]. Likewise the model predicts no significant variation in the mass and energy yield with particle size. The energy yield is predicted to within 3% of the experimental energy yield for all but the smallest particle (r=2.38mm). The discrepancy could be attributed to the fact that the mass loss kinetics and thermochemical submodel are based data from willow while the in this case poplar was used. Unfortunately, the thermochemical data for poplar is lacking so the parameters for willow (a similarly deciduous tree) were used instead.

The trends shown by the model and experimental can not be explained by mere intuition. It would be expected that for a given residence time, larger particles would display *less* conversion (higher mass yield) than smaller particles. A larger particle spends more time heating up

therefore experiences a shorter time at the reaction temperature, and should exhibit lower conversion (higher mass yield). The actual trends can only be explained by examining the predicted conversion profile of the different sized particles. In Figure 4a,b the centerline temperature profile and mass yield are shown for the reactor temperature of 250 and 270 $^{\circ}$C, respectively. Initially, during the heat up period, the larger particles take longer to heat up and dry and therefore displays lower centerline temperatures, and higher mass yields. The centerline of the 12.75mm radius particle takes 30 minutes to reach the 250 $^{\circ}$C reaction temperature while the centerline of the 2.38mm radius particle takes only 6 minutes. During this time, the mass yield shows a strong dependence on particle size. For example at 20 minutes, the mass yield for the largest (12.75mm radius) and smallest (2.38mm radius) particles are 0.905 and 0.985, respectively. However, once the centerline of the particle significantly exceeds 200 $^{\circ}$C (the temperature at which torrefaction reactions initiate), the effect of the exothermic reactions becomes the controlling factor. Since the centerline temperature overshoot increases with particle size, larger particles exhibit higher temperatures and accelerated reaction rates. In the case of 250 $^{\circ}$C, the reactions are accelerated enough so that the difference in mass yield between the large and small particles decreases in time. By t=60 minutes, the difference in conversion between particles of different sizes is very small. Once the thermal overshoot vanishes, the process no longer depends on the particle size (a relatively uniform temperature exists across the particle), and is controlled purely by kinetics.

In the case of 280 $^{\circ}$C (Figure 4b), the exothermic temperature overshoot effects are even larger and although the reactions are accelerated strongly by this effect, the large particles still exhibit *higher* mass yield than the small particles throughout the process. At the end, t=60 minutes, the largest particle (12.75mm radius) exhibits a mass yield nearly the same (0.62) as the

smallest size particle (2.38mm radius) which shows a mass yield of 0.615. In all cases, the behavior of the temperature and conversion profiles can be classified into three different periods: In the first period, the particle heat-up is important and therefore the profiles are governed by the moisture content and heat transfer characteristics of the particle and reactor system. In the second period, the exothermic overshoot effects- which are sensitive to temperature, kinetics, and particle size- become the controlling factor. In the third period, the particle is at uniform temperature and the conversion profile is governed by the mass loss kinetics. The results highlight the importance of coupled, transient models which can account for all three controlling phenomena (heat transfer, thermochemistry, and kinetics).

4.4.Effect of moisture content

In order to understand the effects of moisture content in more detail, a parametric modeling study was completed. The simulation conditions were chosen as representative of those utilized by Basu and co-workers (i.e.initially ambient temperature cylindrical poplar particles dropped into an isothermal reactor at 280 $^{\circ}$C). Only two variables were varied parametrically: particle radius was varied between 2.38 to 12.75 (mm) and initial moisture content from 5 to 30 (%w.b.). In Figure 5a, the heatup time (the time for centerline to reach 200 $^{\circ}$C) is plotted versus the full range of variables simulated). A wide range in the heatup times from as low as 1.2 minutes for the smallest and driest particle (2.38mm,5%w.b) to 35.4 minutes for the largest and wettest (12.75mm,30%w.b) particle is predicted by the model. The heating time varies linearly with moisture content and quadratically with particle size which agrees with results from the experimental drying results Di Blasi [33]. Therefore the larger the particle the more sensitive the length of the drying time is to the initial moisture content. For example, a 10% increase in moisture content lengthens the heatup period for a 12.75mm radius particle by 8 minutes while a

5mm radius particle only takes 2.2 additional minutes for the same increase in moisture content. This sensitivity arises because the drying rate is largely governed by the temperature of the particle which- as discussed previously- depends on the particle size. Overall, the results suggests that when torrefying large (r>10mm) moist particles, attention must be paid to the variations in moisture content between particles which will cause significant variations in conversion even for particles of the exact same size.

In order to demonstrate these sensitivities more clearly, the dry mass yield profiles for two selected particle sizes of 2.38mm and 12.75mm and moisture contents of 5,15,30 %(w.b.) are shown in Figure 5b. For all particles, there is an initial period where the dry mass yield is unchanged (i.e torrefaction reactions have yet to initiate). This delay in the initiation of conversion is attributable to the difference in time needed to heat and dry the particles. For example, the large (12.75mm) and wet (30%) particle takes more than 30 minutes before significant mass loss occurs.

The conversion profile of the 2.38mm particle is largely insensitive to the increased levels of moisture content. For this particle size, throughout the entire 60 minute residence time, at no point does the difference in conversion level (quantified by the mass yield) between the dry (5%w.b.) and the moist (30% w.b.) vary by more than 7 percent. However, the conversion profiles of the large particle (12.75mm) are extremely sensitive to the increasing moisture content. For example, at 35 minutes the dry (5% w.b.) particle is almost completely torreified (the mass yield is <70%) whereas the moist (30% w.b.) particle has yet to undergo significant torrefaction. This further illustrates that grinding of particles prior to torrefaction has a significant advantage: the process becomes much less sensitive to the initial moisture content. Although the temperature profiles aren't shown, the magnitude of the exothermal overshoot is

unaffected by moisture content. This is because the exothermal overshoot does not initiate until the particle is completely dry.

4.5. Implications for reactor design and process control

Several important and novel conclusions regarding the effects of particle size on torrefaction have been elucidated by the present modeling results. Initially, the larger particles take longer than smaller particles to heat up to the reactor temperature. The disparity in time for heat up between small and large particles is exacerbated by increasing moisture content. During this period, conversion decreases strongly with increasing particle size and increasing moisture content. This suggests that it may be advantageous to have a separate grinding and/or drying step prior to the torrefaction process which would help reduce the sensitivity of the process to particle size. During the second phase, the subsequent effect of temperature overshoot caused by exothermic reactions accelerates the conversion of larger particles partially cancelling the effect of the delay caused by their slow heat up. Although the time at which the exothermal overshoot occurs is delayed by increasing moisture content, the magnitude of the overshoot is unaffected by initial moisture content. At the last thermal equilibrium stage of torrefaction, further conversion is governed solely by mass loss kinetics.

The results clearly demonstrate that the torrefaction of small and dry particles will be preferable to large and moist particles because of the former's more rapid and uniform conversion properties. However several economic and energetic trade-offs exists between performing drying and/or grinding prior to the torrefaction process. One solution is to design the torrefaction process itself (for example through modification of the reactor heating conditions) so that the effect of particle size and moisture content on the overall conversion is minimized. While this reduces feedstock pretreatment (i.e grinding, sieving, and drying) costs it may incur

increased reactor complexity and cost. Another factor to consider would be the minimization of the residence time of particles which would reduce the reactor volume and cost. The third overarching constraint is that the process should maximize the energy yield of the solid products. Using the coupled model described here to identify optimal conditions which account for these three competing considerations will be the focus of future work.

5. **Conclusion**

A one-dimensional, coupled model for the torrefaction of single woody biomass particles has been presented and validated against published experimental data. The model is able to predict the thermal behavior as well as the consequent mass and energy yield of initially moist single particles undergoing torrefaction. The results show that the moisture content, particle size, residence time, and reactor temperature have strong and -in some cases nonlinear- effects on the mass and energy yield of the particle. The conversion profiles are characterized by three consecutive stages including (1) particle heat-up and drying, (2) exothermal overshoot, and (3) thermal equilibrium. The length of time required for particle heat-up and drying is determined by the external/internal heat transfer limitations and moisture content. As a result, conversion decreases with increasing particle size and moisture content. During the second exothermal overshoot stage, heat released from chemical reactions causes significant intraparticle gradients and also accelerates the conversion of large particles. While the assumed kinetic and thermochemical parameters are clearly crucial to determining the magnitude of this exothermal overshoot stage, these were not adjusted or tuned during the validation of this particle model. Lastly, when thermal equilibrium is reached, the particle conversion is governed by solely by mass loss kinetics. The validated model can serve as a useful tool in future work to assess the reactor conditions (temperature, residence time) and feed particle sizes necessary to achieve a

homogeneous and sufficient degree of conversion as well as for quantifying the trade-offs between various aspects of the torrefaction process.

Acknolwedgements
The authors gratefully acknowledge BP for funding this research. The authors would also like to thank Dr. Michiel van der stelt for sending a copy of his dissertation.

Sources cited

[1] Bergman PCA, Boersma AR, Kiel JHA, Zwart RWR. Torrefaction for biomass co-firing in existing coal-fired power stations. Energy Research Center of the Netherlands; 2005.

[2] Arias B, Pevida C, Fermoso J, Plaza MG, Rubiera F, Pis JJ. Influence of torrefaction on the grindability and reactivity of woody biomass. Fuel Process Technol 2008;89:169–75.

[3] Prins MJ. Thermodynamic analysis of biomass gasification and torrefaction. Ph.D. thesis. Eindhoven University of Technology, 2005.

[4] Hakkou M, Petrissans M, Gerardin P, Zoulalian A. Investigations of the reasons for fungal durability of heat-treated beech wood. Polym Degrad Stab 2006;91:393–7.

[5] Miao Z, Grift TE, Hansen AC, Ting KC. Energy Requirement for Lignocellulosic Feedstock Densifications in Relation to Particle Physical Properties, Preheating, and Binding Agents. Energy Fuels 2012;27:588–95.

[6] Prins MJ, Ptasinski KJ, Janssen FJJG. Torrefaction of wood: Part 1. Weight loss kinetics. J Anal Appl Pyrolysis 2006;77:28–34.

[7] Peng JH, Bi HT, Sokhansanj S, Lim JC. A Study of Particle Size Effect on Biomass Torrefaction and Densification. Energy Fuels 2012;26:3826–39.

[8] Van der Stelt MJC. Chemistry and reaction kinetics of biowaste torrefaction. Ph.D. thesis. Eindhoven University of Technology, 2011.

[9] Peng JH, Xiaotao TB, Lim J, Sokhansanj S. Development of torrefaction kinetics for British Columbia softwoods. Int J Chem React Eng 2012;10.

[10] Chen W-H, Kuo P-C. Isothermal torrefaction kinetics of hemicellulose, cellulose, lignin and xylan using thermogravimetric analysis. Energy 2011;36:6451–60.

[11] Perré P, Rémond R, Turner I. A comprehensive dual-scale wood torrefaction model: Application to the analysis of thermal run-away in industrial heat treatment processes. Int J Heat Mass Transf 2013;64:838–49.

[12] Chan W-CR, Kelbon M, Krieger BB. Modelling and experimental verification of physical and chemical processes during pyrolysis of a large biomass particle. Fuel 1985;64:1505–13.

[13] Di Blasi C. Physico-chemical processes occurring inside a degrading two-dimensional anisotropic porous medium. Int J Heat Mass Transf 1998;41:4139–50.

[14] Grønli MG, Melaaen MC. Mathematical Model for Wood Pyrolysis: Comparison of Experimental Measurements with Model Predictions. Energy Fuels 2000;14:791–800.

[15] Lu H, Ip E, Scott J, Foster P, Vickers M, Baxter LL. Effects of particle shape and size on devolatilization of biomass particle. Fuel 2010;89:1156–68.

[16] Haseli Y, van Oijen JA, de Goey LPH. Numerical study of the conversion time of single pyrolyzing biomass particles at high heating conditions. Chem Eng J 2011;169:299–312.

[17] Turner I, Rousset P, Remond R, Perre P. An experimental and theoretical investigation of the thermal treatment of wood (Fagus sylvatica L.) in the range 200-260C. Int J Heat Mass Transf 2010;53:715–25.

[18] Kadem S, Lachemet A, Younsi R, Kocaefe D. 3d-Transient modeling of heat and mass transfer during heat treatment of wood. Int Commun Heat Mass Transf 2011;38:717–22.

[19] Patuzzi F, Gasparella A, Baratieri M. Thermochemical and Fluid Dynamic Model of a Bench-Scale Torrefaction Reactor. Waste Biomass Valorization 2013:1–9.

[20] Ratte J, Marias F, Vaxelaire J, Bernada P. Mathematical Modelling of Slow Pyrolysis of a Particle of Impregnated Wood. High Temp Mater Process 2008;27:291–390.

[21] Ratte J, Fardet E, Mateos D, Héry J-S. Mathematical modelling of a continuous biomass torrefaction reactor: TORSPYD^{TM} column. Biomass Bioenergy 2011;35:3481–95.

[22] Basu P, Sadhukhan AK, Gupta P, Rao S, Dhungana A, Acharya B. An experimental and theoretical investigation on torrefaction of a large wet wood particle. Bioresour Technol 2014;159:215–22.

[23] Basu P, Rao S, Dhungana A. An investigation into the effect of biomass particle size on its torrefaction. Can J Chem Eng 2013;91:466–74.

[24] Francescato V, Antonini E, Bergomi L. Wood Fuels Handbook. AIEL Italian Agriforestry Energy Association; 2008.

[25] Bergman R. Drying and control of moisture content and dimensional changes. In: Cai Z, Carll C, Clausen C, Dietenberger M, Falk R, editors. Wood Handb. Wood Eng. Mater., Madison, WI: USDA Forest Service; 2010, p. 1–20.

[26] Pirraglia A, Gonzalez R, Saloni D. Technoeconomical analysis of wood pellets production for US manufacturers. Bioresources 2010;5:2374–90.

[27] Di Blasi C. Simultaneous Heat, Mass and Momentum Transfer during Biomass Drying. In: Bridgwater AV, Boocock DGB, editors. Dev. Thermochem. Biomass Convers., Springer Netherlands; 1997, p. 117–31.

[28] Basu P. Biomass gasification and pyrolysis: Practical design and theory. Massachusetts: Academic Press; 2010.

[29] Grønli MG. A theoretical and experimental study of the thermal degradation of biomass. Ph.D. thesis. Norwegian University of Science and Technology, 1996.

[30] Bridgeman TG, Jones JM, Shield I, Williams PT. Torrefaction of reed canary grass, wheat straw and willow to enhance solid fuel qualities and combustion properties. Fuel 2008;87:844–56.

[31] Pimchuai A, Dutta A, Basu P. Torrefaction of Agriculture Residue To Enhance Combustible Properties†. Energy Fuels 2010.

[32] Tumuluru JS, Sokhansanj S, Wright CT, Boardman RD. Biomass torrefaction process review and moving bed torrefaction system model development. Idaho Falls, Idaho: Idaho National Lab; 2010.

[33] Di Blasi CD, Branca C, Sparano S, La Mantia B. Drying characteristics of wood cylinders for conditions pertinent to fixed-bed countercurrent gasification. Biomass Bioenergy 2003;25:45–58.

[34] Alves SS, Figueiredo JL. A model for pyrolysis of wet wood. Chem Eng Sci 1989;44:2861–9.

[35] Babu BV, Chaurasia AS. Heat transfer and kinetics in the pyrolysis of shrinking biomass particle. Chem Eng Sci 2004;59:1999–2012.

[36] Parker WJ. Development of a model for the heat release rate of wood: A status report. 1985.

[37] Pyle DL, Zaror CA. Heat transfer and kinetics in the low temperature pyrolysis of solids. Chem Eng Sci 1984;39:147–58.

[38] Grieco E, Baldi G. Analysis and modelling of wood pyrolysis. Chem Eng Sci 2011;66:650–60.

[39] Galgano A, Di Blasi C. Modeling the propagation of drying and decomposition fronts in wood. Combust Flame 2004;139:16–27.

[40] Porteiro J, Míguez JL, Granada E, Moran JC. Mathematical modelling of the combustion of a single wood particle. Int Congr Energy Environ Eng Manag 2006;87:169–75.

[41] Krieger-Brockett B, Glaister D. Wood Devolatilization - Sensitivity to Feed Properties and Process Variables. In: Bridgwater AV, Kuester JL, editors. Res. Thermochem. Biomass Convers., Springer Netherlands; 1988, p. 127–42.

[42] Shrestha S, Cramer S, White R. Time temperature profiles across a lumber section exposed to pyrolytic temperatures. Fire Mater 1994;18:211–20.

[43] Bryden KM, Ragland KW, Rutland CJ. Modeling thermally thick pyrolysis of wood. Biomass Bioenergy 2002;22:41–53.

[44] Wurzenberger JC, Wallner S, Raupenstrauch H, Khinast JG. Thermal conversion of biomass: Comprehensive reactor and particle modeling. AIChE J 2002;48:2398–411.

[45] Lu H, Robert W, Peirce G, Ripa B, Baxter LL. Comprehensive Study of Biomass Particle Combustion. Energy Fuels 2008;22:2826–39.

[46] Ouelhazi N, Arnaud G, Fohr JP. A two-dimensional study of wood plank drying. The effect of gaseous pressure below boiling point. Transp Porous Media 1992;7:39–61.

[47] Peters B, Schröder E, Bruch C, Nussbaumer T. Measurements and particle resolved modelling of heat-up and drying of a packed bed. Biomass Bioenergy 2002;23:291–306.

[48] Bilbao R, Mastral JF, Ceamanos J, Aldea ME. Modelling of the pyrolysis of wet wood. J Anal Appl Pyrolysis 1996;36:81–97.

[49] Saastamoinen J, Richard J-R. Simultaneous drying and pyrolysis of solid fuel particles. Combust Flame 1996;106:288–300.

[50] Aerts PD., Ragland KW. Pressurized downdraft combustion of woodchips. Twenty-Third Symp Int Combust 1991;23:1025–32.

[51] Bellais M. Modelling of the pyrolysis of large wood particles. PhD thesis. KTH Royal Institute of Technology, 2007.

[52] Peters B, Bruch C. A flexible and stable numerical method for simulating the thermal decomposition of wood particles. Proc 6th Intl Congr Toxic Combust 2001;42:481–90.

[53] Alverez Noves H, Fernandez-Golfin Seco JI. Practical evaluation and operation of superheated steam drying process with different softwoods and hardwoods. Eur J Wood Wood Prod 1994;52:135–8.

[54] Nocquet T, Dupont C, Commandre J-M, Grateau M, Thiery S, Salvador S. Volatile species release during torrefaction of wood and its macromolecular constituents: Part 1 – Experimental study. Energy 2014;(In press).

[55] Cavagnol S, Sanz E, Nastoll W, Roesler JF, Zymla V, Perré P. Inverse analysis of wood pyrolysis with long residence times in the temperature range 210–290 °C: Selection of multi-step kinetic models based on mass loss residues. Thermochim Acta 2013;574:1–9.

[56] Di Blasi C, Lanzetta M. Intrinsic kinetics of isothermal xylan degradation in inert atmosphere. J Anal Appl Pyrolysis 1997;40-41:287–303.

[57] Bates RB, Ghoniem AF. Biomass torrefaction: Modeling of volatile and solid product evolution kinetics. Bioresour Technol 2012;124:460–9.

[58] Bates RB, Ghoniem AF. Biomass torrefaction: Modeling of reaction thermochemistry. Bioresour Technol 2013;134:331–40.

[59] Joshi Y, de Vries H, Woudstra T, de Jong W. Torrefaction: Unit Operation Modelling and Process Simulation. Appl Therm Eng 2014;(In Press).

[60] Scott SA, Davidson JF, Dennis JS, Hayhurst AN. The devolatilisation of particles of a complex fuel (dried sewage sludge) in a fluidised bed. Chem Eng Sci 2007;62:584–98.

[61] Nowak W, Stachel AA. Convective heat transfer in air flow around a cylinder at low Reynolds numbers. J Eng Phys Thermophys 2005;78:1214–21.

[62] Milosavljevic I, Oja V, Suuberg EM. Thermal Effects in Cellulose Pyrolysis: Relationship to Char Formation Processes. Ind Eng Chem Res 1996;35:653–62.

[63] Rath J, Steiner G, Wolfinger M., Staudinger G. Tar cracking from fast pyrolysis of large beech wood particles. J Anal Appl Pyrolysis 2002;62:83–92.

[64] Dhungana A. Torrefaction of biomass. Master's thesis. Dalhousie University, 2011.

[65] Basu P, Rao S, Acharya B, Dhungana A. Effect of torrefaction on the density and volume changes of coarse biomass particles. Can J Chem Eng 2013;91:1040–4.

[66] Merrick D. Mathematical models of the thermal decomposition of coal: 2. Specific heats and heats of reaction. Fuel 1983;62:540–6.

[67] Boie W. Fuel technology calculations. Energitechnik 1953;3:309–16.

Figure Captions

Figure 1 Centerline and near surface temperature versus time for r=0.014m beech particles at final reactor temperatures of 235 and 289 $^{\circ}$C for a) and c), respectively. Intraparticle temperatures for respective cases shown in b) and d) at t=10,20,40 minutes Experimental data from van der stelt [8]

Figure 2 Effect of final reactor temperature on centerline temperature overshoot (a) and final (t=60 minutes) mass/energy yields (b) for a 14mm radius beech cylinder initially at 20.5°C exposed to 10 $^{\circ}$C/min reactor heating rate, and a 27 $^{\circ}$C initial reactor temperature. Experimental data in a) from van der Stelt **[8].**

Figure 3 Effect of the particle size on the centerline-reactor temperature overshoot (a) Particle size versus heat-up time (b) Mass/energy yields versus particle size (c). Experimental data from Basu et al. 2013 [23], reactor temperature=250 $^{\circ}$C

Figure 4 Centerline temperature versus time (minutes) left axis for various particle sizes (radius=2.38, 5, 7.5, 12.75 mm). Mass yield versus time (right axis) Reactor temperature =250, 280 $^{\circ}$C for a),b) respectively.

Figure 5 a) Heatup time versus wet basis moisture content (%) b) Dry mass yield versus time for two different particle sizes (R=2.38,12.75mm), and three different initial moisture contents (5,15,30% w.b).

Table Titles

Table 1 Characteristic times of physical and chemical processes occurring during torrefaction

Table 2 Assumed thermodynamic and physical properties for single particle torrefaction simulation

Tables and Figures

Table 1 Characteristic times of physical and chemical processes occurring during torrefaction

	Characteristic time (s)	
	T= 300 °C	
Transport process or reaction	Microscale L=10 μm	Macroscale L=1 cm
Diffusion, L^2/D_{eff}	10^{-6}	10
Intraparticle fluid flow, $\mu L^2/pB_0$	10^{-5}	1
Convective/Radiative Heat Transfer, $(\rho c_p)_s L/h$	10^{-1}	10^3
Conduction Heat Transfer, $(\rho c_p)_s L^2/k$	10^{-4}	10^2
Torrefaction mass loss kinetics, $1/k_1$	10^2	10^2
Drying kinetics $1/k_d$	10^2	10^2

$D_{eff} \approx 10^{-6}$ m^2 s^{-1}	$B_0 \approx 10^{-14}$ m^2
$(\rho c_p)_s \approx 10^6$ J m^{-3} K^{-1}	$h \approx 10$ W m^2 K^{-1}
$(\rho c_p)_g \approx 10^4$ J m^{-3} K^{-1}	$k \approx 10^{-1}$ W m K^{-1}
$\mu \approx 10^{-5}$ Pa s	$k_1 \approx 239$ s^{-1}
$\Delta p \approx 10^4$ Pa	$k_d \approx 440$ s^{-1}

Table 2 Assumed thermodynamic and physical properties for single particle torrefaction simulation

Property	Correlation/Value	Source
Dry wood density	$\rho_{A0} = \rho_{s0} = 700{,}500\ kg\ m^{-3}$ *(Beech, Poplar)*	[29,65]
Initial wood composition (dry basis)	$Y_{j,S0} = 0.4692, 0.0585, 0.4662, 0.0001, 0.006$ *(Beech) for j=C,H,O,N,Ash* $Y_{j,S0} = 0.4845, 0.0585, 0.4369, 0.0047, 0.0143$ *(Poplar)*	[8] [23]
Solid specific heat capacity	$cp_i = \frac{R}{MW_i}\left[e^{\frac{380}{T}}\left(\frac{e^{\frac{380}{T}}-1}{\frac{380}{T}}\right)^{-2} + 2e^{\frac{1800}{T}}\left(\frac{e^{\frac{1800}{T}}-1}{\frac{1800}{T}}\right)^{-2}\right]\ J\ kg^{-1}K^{-1}$	[66]
Solid average molecular weight	$MW_i = \left[\sum_{j=1}^{5}\frac{Y_j}{MW_j}\right]^{-1}$ *i=A,B,C* $j = C, H, O, N$ $kg\ mol^{-1}$	[66]
Solid higher heating value	$HHV_i = 1000[351.69(Y_C) + 1162.46(Y_H) - 110.95(Y_O) + 104.67(Y_S) - 62.8(Y_N)]\ J\ kg^{-1}$	[67]
Solid standard heat of formation	$H^{\circ}_{f,i} = HHV_i + \frac{Y_H}{2MW_H}H^{\circ}_{f,H_2O(l)} + \frac{Y_C}{MW_C}H^{\circ}_{f,CO_2}$ *i=A,B,C,S* $J\ kg^{-1}$	[58]
V1 specific heat capacity	$cp_{V1} = 1162 + 0.961T\ J\ kg^{-1}K^{-1}$	[58]
V2 specific heat capacity	$cp_{V2} = 601 + 2.262T\ J\ kg^{-1}K^{-1}$	[58]
V1 standard heat of formation	$H^{\circ}_{f,V1} = -10{,}345{,}151\ J\ kg^{-1}$	[58]
V2 standard heat of formation	$H^{\circ}_{f,V1} = -7{,}078{,}295\ J\ kg^{-1}$	[58]
Heat of vaporization	$\Delta H^{\circ}_{evap} = -2{,}260{,}000\ J\ kg^{-1}$ for $MC_d > M_{fsp}$ $\Delta H^{\circ}_{evap} = 10^6[3.348 - 13.085(MC_d) + 60.262(MC_d)^2 - 95.778(MC_d)^3]\ J\ kg^{-1}$ for $MC_d < M_{fsp}$	[48]
Wood thermal conductivity	$k_A = 0.209, 0.11\ W\ m^{-1}\ K^{-1}$ *(Beech,Poplar)*	[15,29]
Torrefied phase (B) thermal conductivity	$k_B = (k_A + k_C)/2\ W\ m^{-1}\ K^{-1}$	*(Estimated)*
Char (C) thermal conductivity	$k_C = 0.071\ W\ m^{-1}\ K^{-1}$ *(Beech,Poplar)*	[15,29]
Moisture thermal conductivity	$k_{MC} = (0.406\ MC_d)\ \rho_{S0}/1000\ W\ m^{-1}\ K^{-1}$	[43]
Effective thermal conductivity	$k_{eff} = (\rho_A k_A + \rho_B k_B + \rho_C k_C)/\rho_{A0} + k_{MC} + \varepsilon k_{gas} + 13.5\ \sigma d T^3/\omega\ W m^{-1}\ K^{-1}$	[12]
Gas thermal conductivity	$k_{gas} = 25.77 * 10^{-3}\ W\ m^{-1}\ K^{-1}$	[13]
Emissivity coefficient	$\omega = 0.95$	[35]
Porosity	$\varepsilon = 1 - (1 - \varepsilon_0)(\rho_A + \rho_B + \rho_C)/\rho_{A0}$	*[35]*
Pore diameter	$d = 2 * 10^{-5}\ m$	[35]
Stefan-Boltzmann constant	$\sigma = 5.67 * 10^{-8}$ W $m^{-2}K^{-4}$	
Kinetic rate parameters k_1 *(A→B)*	$2.48 * 10^4\ exp(-75976/RT)\ s^{-1}$	[6]
k_{V1} *(A→V1)*	$3.23 * 10^7\ exp(-114214/RT)\ s^{-1}$	
k_2 *(B→C)*	$1.1 * 10^{10}\ exp(-151711/RT)\ s^{-1}$	
k_{V2} *(B→V2)*	$1.59 * 10^{10}\ exp(-151711/RT)\ s^{-1}$	
Drying parameters k_d *(MC_{liq}→MC_{vap})*	$4.5 * 10^3\ exp(-45000/RT)\ s^{-1}$	[36]
Vaporization temperature	$T_b = 73.204\ exp(26.451 MC_d) + 373\ K$	*Fitted from* [53]

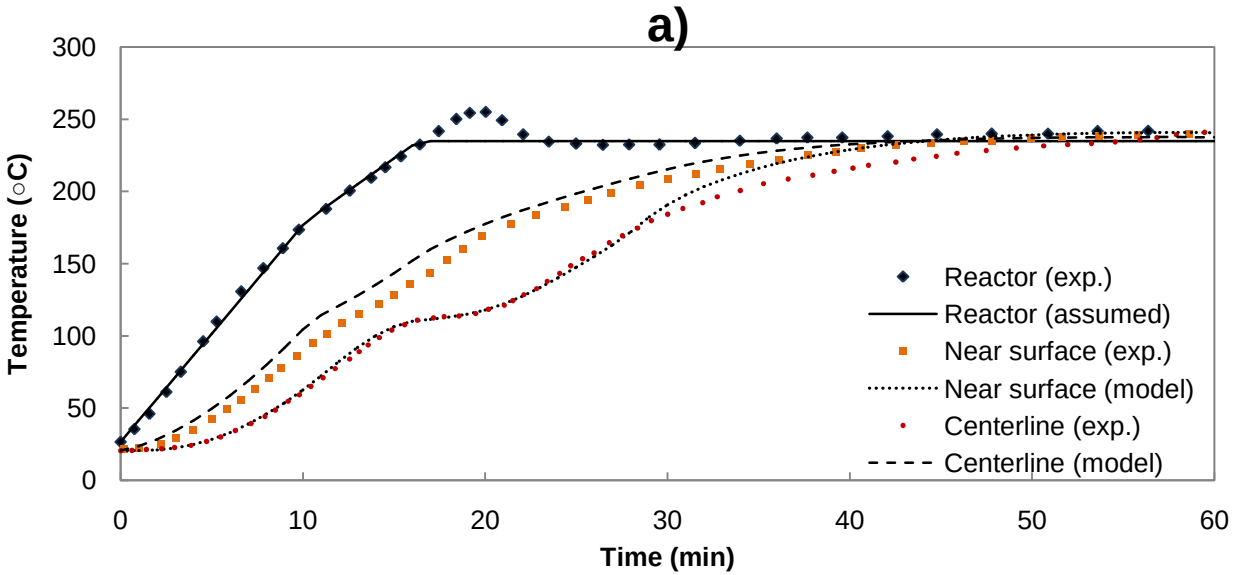
a)
Temperature (○C)
300
250
200
150
100
50
0
0
10
20
30
40
50
60
Time (min)
Reactor (exp.)
Reactor (assumed)
Near surface (exp.)
Near surface (model)
Centerline (exp.)
Centerline (model)

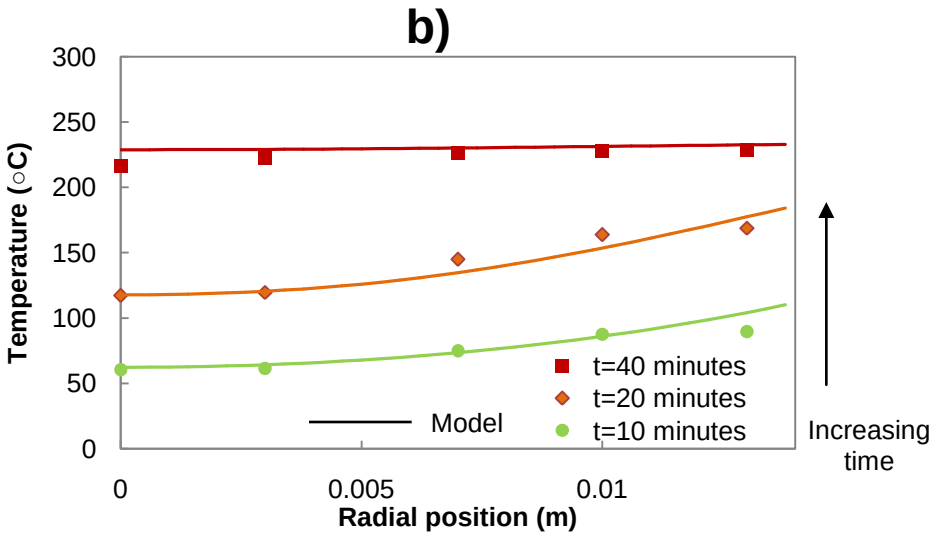
b)
Temperature (○C)
300
250
200
150
100
50
0
0
0.005
0.01
Radial position (m)
t=40 minutes
t=20 minutes
t=10 minutes
Model
Increasing time

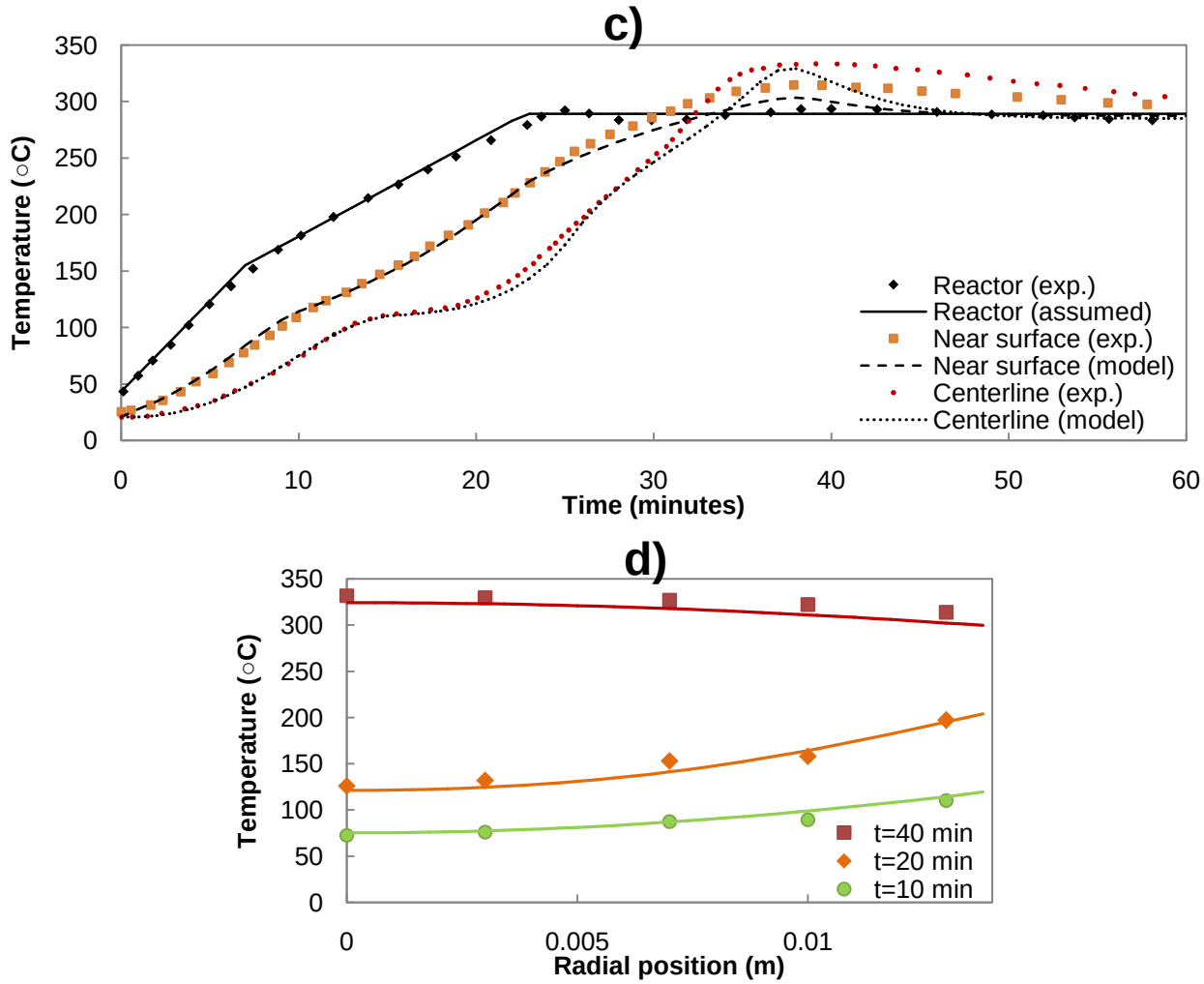

Figure 1 Centerline and near surface temperature versus time for r=0.014m beech particles at final reactor temperatures of 235 and 289 °C for a) and c), respectively. Intraparticle temperatures for respective cases shown in b) and d) at t=10,20,40 minutes Experimental data from van der stelt [8]

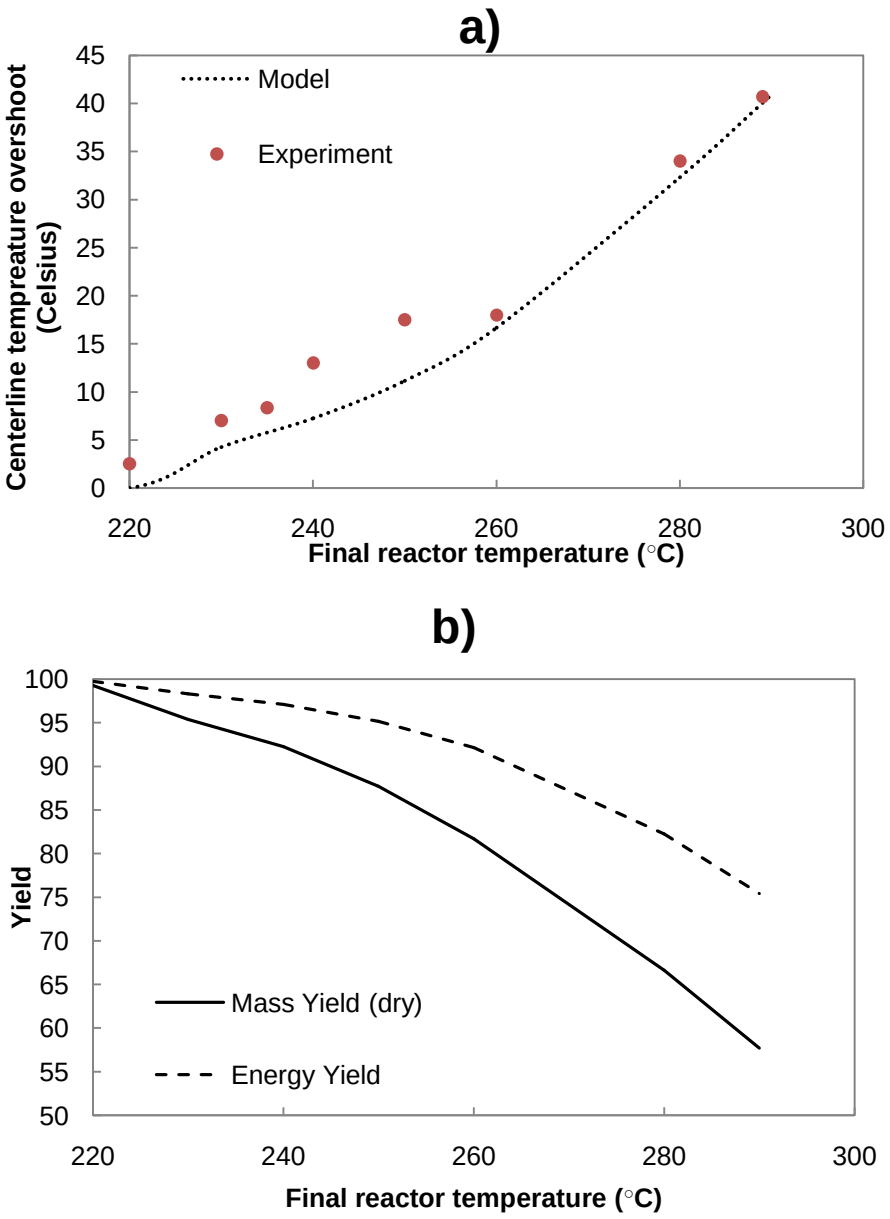

Figure 2 Effect of final reactor temperature on centerline temperature overshoot (a) and final (t=60 minutes) mass/energy yields (b) for a 14mm radius beech cylinder initially at 20.5°C exposed to 10 °C/min reactor heating rate, and a 27 °C initial reactor temperature. Experimental data in a) from van der Stelt [8].

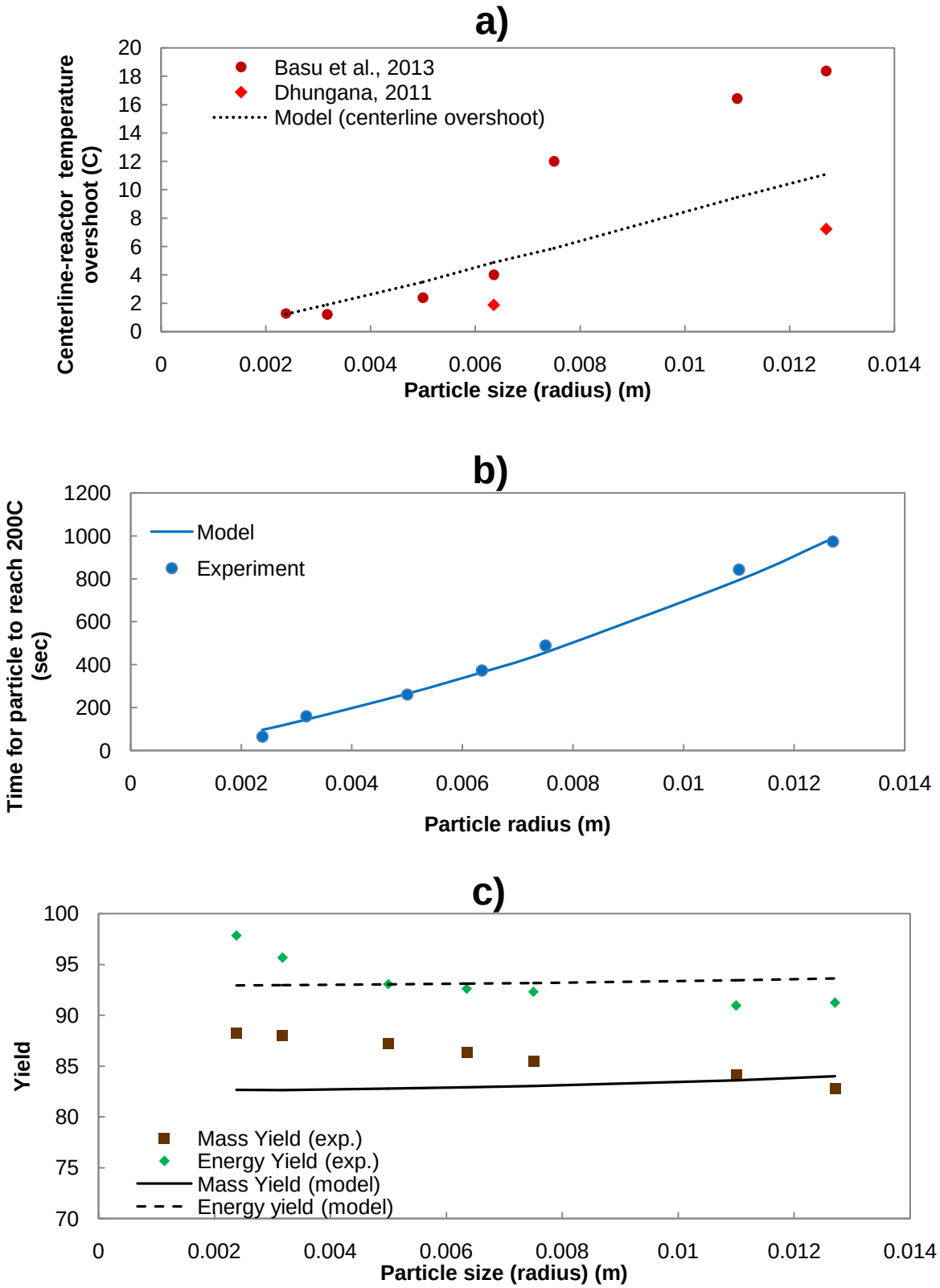

Figure 3 Effect of the particle size on the centerline-reactor temperature overshoot (a) Particle size versus heat-up time (b) Mass/energy yields versus particle size (c). Experimental data from Basu et al. 2013 [23], reactor temperature=250 °C

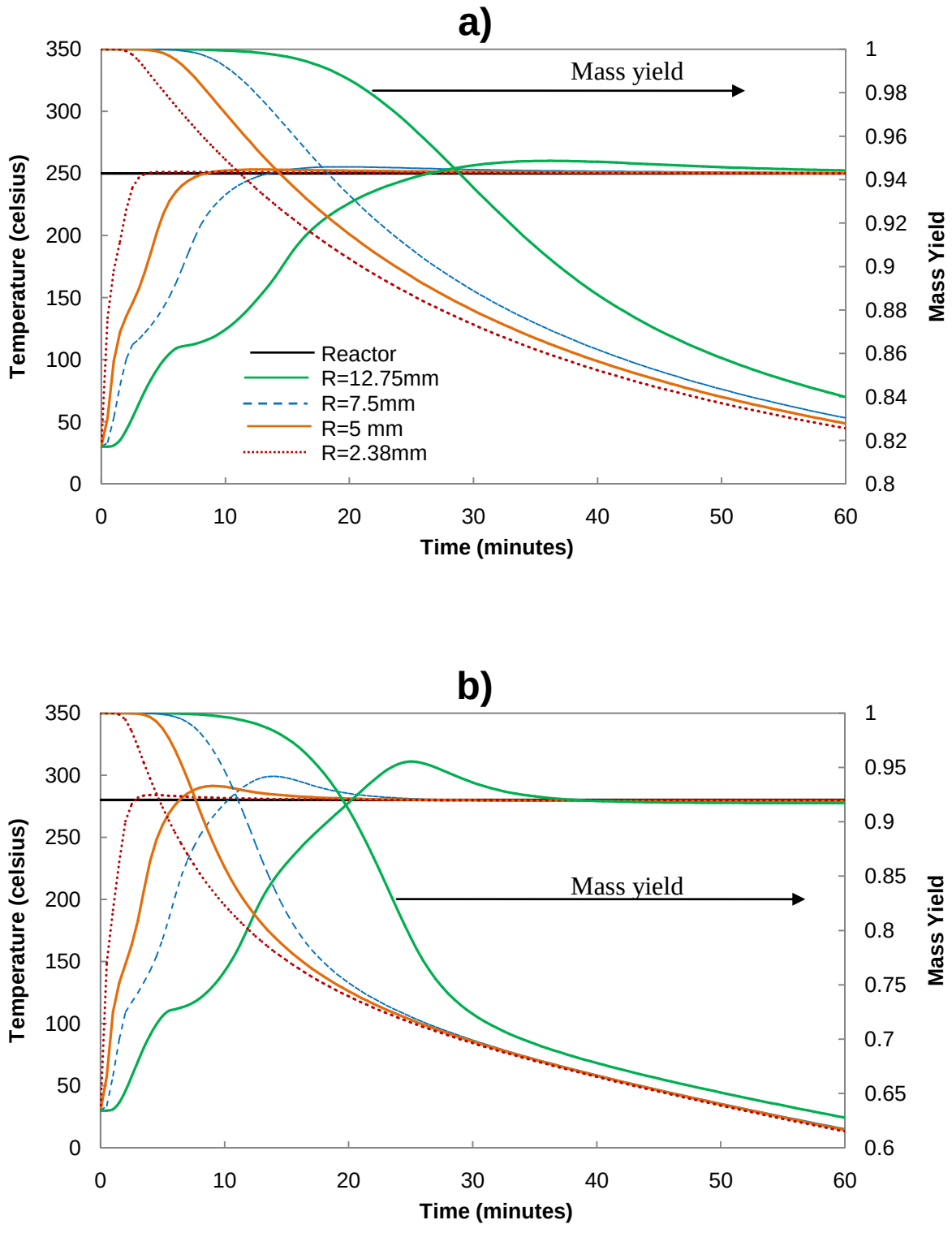

Figure 4 Centerline temperature versus time (minutes) left axis for various particle sizes (radius=2.38, 5, 7.5, 12.75 mm). Mass yield versus time (right axis) Reactor temperature =250, 280 °C for a),b) respectively.

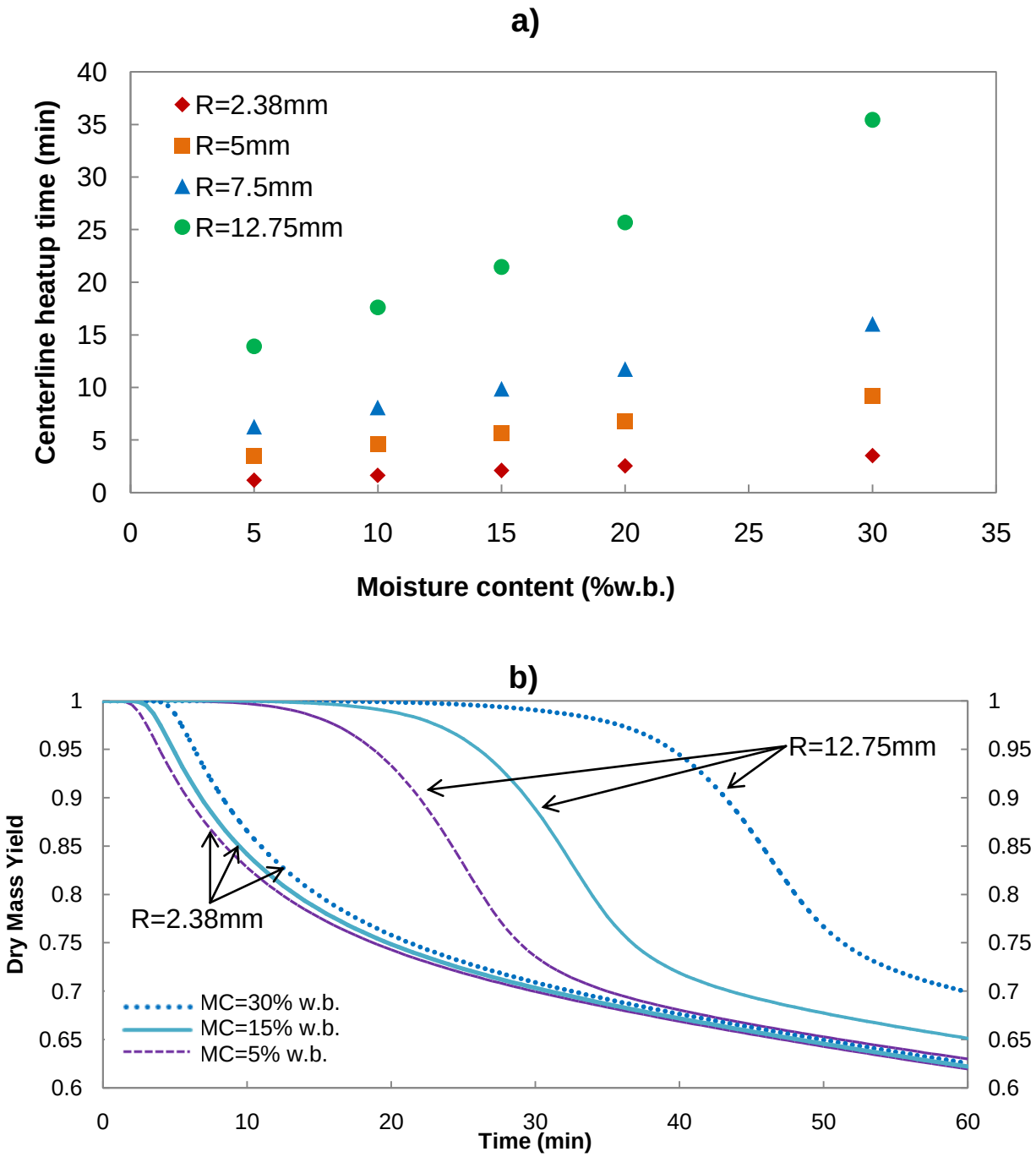

Figure 5 a) Heatup time versus wet basis moisture content (%) b) Dry mass yield versus time for two different particle sizes (R=2.38,12.75mm), and three different initial moisture contents (5,15,30% w.b).